PNAS
www.pnas.org

Supplementary Information for

Acid-sensing ion channels emerged over 600 Mya and are conserved throughout the deuterostomes

Timothy Lynagh, Yana Mikhaleva, Janne M. Colding, Joel C. Glover, Stephan A. Pless

Correspondence to Timothy Lynagh
Email: tplynagh@gmail.com

This PDF file includes:

Supplementary text
Fig. S1 to S6
References for supplementary information

www.pnas.org/cgi/doi/10.1073/pnas.1806614115

Supplementary text

Materials and Methods

Sequence assembly and phylogenetic analysis. To establish phylogenetic DEG/ENaC relationships throughout the deuterostomes, DEG/ENaC amino acid sequences were sought from one vertebrate (*Mus musculus*), one tunicate (*Oikopleura dioica*), two cephalochordates (*Branchistoma belcheri* and *Branchiostoma floridae*; closely related but the only cephalochordate data available), two echinoderms (*Strongylocentrotus purpuratus* and *Acanthaster planci*) and two hemichordates (*Ptychodera flava* and *Saccoglossus kowalevskii*). Sequences were retrieved through blastp (tblastn yielded similar results) using the mouse ASIC1a amino acid sequence in Oikobase (*O. dioica*, http://oikoarrays.biology.uiowa.edu/Oiko/), OIST Marine Genomics Unit (*A. planci* and *P. flava*, http://marinegenomics.oist.jp/acornworm/gallery), and NCBI (for all others, https://blast.ncbi.nlm.nih.gov). After initial alignment using MAFFT v7.017 (1), removal of >99% identical, redundant sequences and removal of obviously incomplete sequences, sequences were re-aligned with MAFFT and poor-aligning segments and/or numerous gaps were removed manually. The result was an alignment of 102 sequences with 299 amino acid positions, from before the first membrane-spanning helix (M1) to the end of the second (M2). This alignment was used to generate maximum likelihood trees with PHYML (2) using either LG or WAG models of evolution, as indicated in figure legends, both with variable substitution rate parameter, Γ, estimated. Branch support was estimated through 100 replicates. To compare with protostome sequences, the 102 deuterostome sequences were aligned with sequences from two major protostome lineages, Ecdysozoa and Spiralia: seven arthropod (*Centruroides sculpturatus*) and 16 mollusk (*Lottia gigantea*) sequences were retrieved from blastp searches (with mouse ASIC1a) at NCBI and the Joint Genome Institute (https://genome.jgi.doe.gov/Lotgi1/Lotgi1.home.html), respectively. A search for DEG/ENaC sequences in Xenacoelomorpha (the sister group to dueterostomes and protostomes (3)) retrieved no results. In assessing ASIC4 phylogeny, vertebrate sequences were retrieved from NCBI with blastp using rat ASIC4. This initially retrieved numerous redundant and non-ASIC4 sequences, which were removed through preliminary alignments (MAFFT) and trees (FastTree v2.1.5 (4)) including mouse ASIC1a, ASIC2a, ASIC3 and BASIC to identify and remove any non-ASIC4 sequences (not shown). Subsequently, sequences were re-aligned, 36 mammalian sequences were removed to avoid bias, gaps were manually removed and an alignment of 108 sequences and 390 positions was used to generate a maximum likelihood tree in PHYML (LG + Γ). All alignments and trees were performed as plugins within Geneious v8.1.8 (5). Deuterostome DEG/ENaC alignment and vertebrate ASIC4 alignment are available at Dryad Digital Repository under doi:10.5061/dryad.46320g1.

ASIC cDNA synthesis and expression. Sequences chosen for cDNA synthesis, cRNA transcription and expression were *O. dioica* 00000722001 and *B. belcheri* XP_019621273 (Group A ASICs); and *B. belcheri* XP_019623542.1 (see below for more detail), *P. flava* 1g14838, *S. purpuratus* XP_780968.2, and *A. planci* gbr.173.6.t1 (Group B ASICs). These were selected primarily based on their position throughout the ASIC clade (orange in Fig. 1A) and their representation of each deuterostome lineage, however another criteria for selection was apparent full length as compared with mouse ASIC1a. *B. belcheri* XP_019623542.1 was obviously incomplete, but phylogenetic analysis suggested it is orthologous to *B. floridae* 85006 (Fig. S1C), and by combining these sequences we generated "*B. belcheri* Group B^{Chi}" a chimeric sequence representing this branch of the ASIC clade. A nine amino acid 1D4 tag (6); nucleotide sequence ACCGAGACCTCTCAAGTGGCTCCAGCT) was inserted before the final stop codon in all sequences in case subsequent protein purification was required. ASIC4 sequences were selected similarly (from tree in Fig. 4A), including *Latimeria chalumnae* (coelacanth) ASIC4 XP_005995842.1 (cDNA XM_005995780.1), *Xenopus laevis* (frog) ASIC4 XP_018091197.1 (cDNA HM137020.1) and *Gallus gallus* (chick) ASIC4 XP_015145601.1 (cDNA XM_015290115.1). The 1D4 tag was also inserted in these ASIC4 sequences. Rat ASIC4/mouse ASIC1a chimera design is summarized in Fig. S4. Each of the above DNAs was commercially synthesized and sub-cloned into the pSP64 (polyA) vector between XbaI (ASIC4/ASIC1a chimeras) or BamHI (all others) and SacI sites (Invitrogen GeneArt; Thermo Fisher Scientific), which were silently mutated out of the coding sequences, if required. Mouse ASIC1a (in pSP64) was provided by Marcelo Carratino (University of Pittsburgh), and rat ASIC4 (in pRSSP6009) and zebrafish ASIC4.1 (in pRSSP6009)

clones were provided by Stefan Gründer (RWTH Aachen University). All newly characterized cDNA sequences are available at Dryad Digital Repository under doi:10.5061/dryad.46320g1.

Site-directed mutagenesis was performed with standard PCR using PfuUltraII Fusion polymerase (Agilent) and custom DNA mutagenesis primers (Eurofins Genomics), or, for insertion and deletion constructs, with the Q5 site-directed mutagenesis kit (New England Biolabs). All sequences, mutant and WT, were confirmed by sequencing of the full insert (GATC Biotech). cDNAs were linearized with MluI (rat ASIC4 and zebrafish ASIC4.1) or EcoRI (all other constructs; New England Biolabs) and capped cRNA was transcribed with the Ambion mMESSAGE mMACHINE kit (Thermo Fisher Scientific).

Electrophysiological recordings and data analysis. *Xenopus laevis* oocytes were prepared as previously described (7) under license 2014-15-0201-00031 from the Danish Veterinary and Food Administration. Oocytes were injected with 0.8 ng cRNA (WT and regular site-directed mutant mouse ASIC1a constructs, unless indicated otherwise in figure legends), 4 ng cRNA (most deletion-mutant mouse ASIC1a constructs; WT and deletion-mutant invertebrate ASIC constructs; and ncAA-containing mouse ASIC1a), or 40 ng cRNA (ΔH73 and ΔK211 mouse ASIC1a; ΔH109 and ΔK250 *B. belcheri* Group B ASIC (see Fig. 2B,C); cysteine-mutant mASIC1a constructs (see Fig. 2E,F); all ASIC4 constructs; and rat ASIC4/mouse ASIC1a chimeras). ncAA incorporation was performed as previously described (8) and is briefly summarized in Fig. S3D legend.

1-3 days after injection, oocytes were transferred to a recording chamber (9), continuously perfused with bath solution containing (in mM): 96 NaCl, 1 KCl, 1.8 $CaCl_2$, 1 $MgCl_2$, and 5 HEPES (for pH > 6.0) or 5 MES (for pH ≤ 6.0). pH was adjusted with NaOH, HCl, or KOH, as appropriate. For ion selectivity experiments, NaCl was replaced with KCl (see Fig. S2A). In most experiments, acidic pH was applied to oocytes in between resting periods (pH 7.5 unless otherwise indicated) of approximately 30 s (or longer, as indicated in figures).

Two-electrode voltage clamp recordings used an OC-725C amplifier (Warner Instruments), Digidata 1550 digitizer (Molecular Devices) and pClamp v10.6 software (Molecular Devices). Currents were acquired at 1 kHz and filtered at 200 Hz (and 1 Hz for display in figures). Oocytes were clamped at -40 mV for ASIC1a and invertebrate ASIC experiments and at -60 mV for ASIC4 experiments. The measurement of ion selectivity is described in Fig. S2A.

After retrieving current amplitude from pClamp, all data analyses were performed in Prism v6 or v7 (GraphPad Software). For proton concentration-response data, peak current amplitude was plotted against pH and fitted with the Hill equation for each recording. These were averaged to give the reported means ± SD in the main text and in Table 1. For display in figures, a single fit to the average normalized responses (± SEM) is shown. Multiple comparisons were made with one-way analysis of variance with Dunnett's comparison to a control value (e.g. comparing with WT) or with Tukey's test for multiple comparisons.

Synthesis of RNA probes for *in situ* hybridization (ISH). Two PCR products of different length were obtained from sscDNA. Primers used for probe synthesis were:
ASIC-sense: GCTTCAAATGTTACTATGCATGG and
ASIC-anti-sense 1: GCTTCGTATGTGATCTCGTCCGAT,
ASIC-anti-sense 2: TATCTGCACACTGATACTGTTTGG.
PCR products were cloned into pGemT-easy vector (A1360, Promega) and sequenced before *in vitro* transcription. Probes were labeled with DIG-labeling mix (Roche).

Whole mount ISH. The ISH protocol was as described in (10). The same ISH pattern was obtained using either anti-sense probe (698bp and 1021bp). Specimens were imaged using a Nikon Eclipse E800 compound microscope (40x objective) and photographed with a Nikon Digital Sight DSU3 camera. Figures were composed using Adobe Photoshop CS5, employing some cropping and adjustment of brightness/contrast. All such adjustments were applied equivalently to the entire image, and did not alter the pattern or location of the ISH signal.

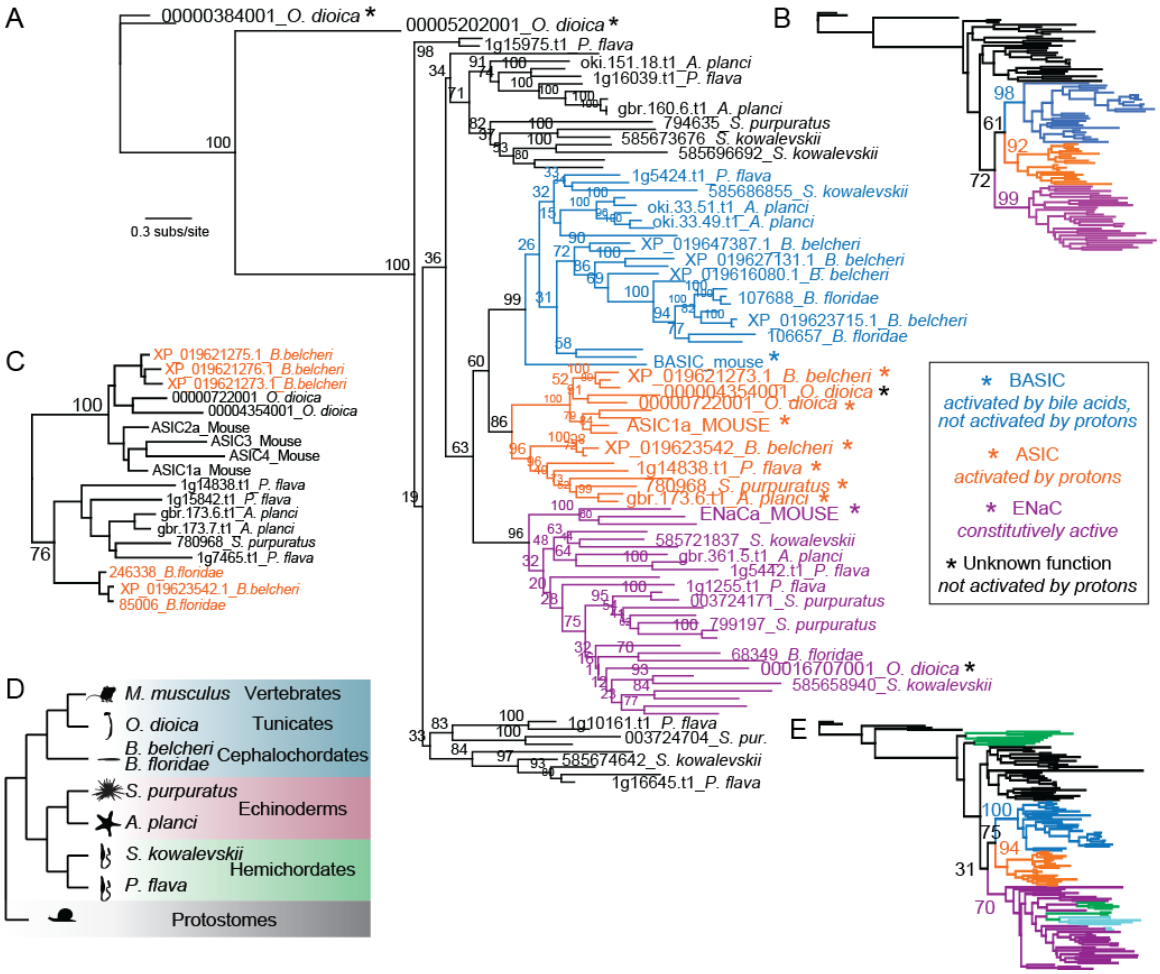

Fig. S1. Phylogenetic analysis of deuterostome DEG/ENaC subunits. (A) Maximum likelihood tree (PHYML, LG + Γ; branch labels show bootstrap support from 100 replicates) inferred from alignment of 102 DEG/ENaC amino acid sequences from one vertebrate, one tunicate, two cephalochordates, two echinoderms and two hemichordates (for details on sequence sources, see *Materials and Methods, Sequence assembly and phylogenetic analysis*). Color-coded asterisks refer to experimental evidence of indicated function, either from previous studies (11, 12) or from additional *O. dioica* clones that were synthesized and tested in the present study (black asterisks). (B) PHYML tree using WAG + Γ model. Bootstrap support (/100) shown for selected branches. Colors as in (A). This shows that WAG and LG models return the same key branches. (C) Tree based on alignment of fewer amino acids, using only the amino acids available in both *B. belcheri* XP_019623542 and *B. floridae* 85006. Like the larger alignments, this supports the position of these sequences in Group B. (*B. floridae* 246338 was removed from the alignment/tree in Fig. 1A due to missing N-terminal data.) (D) Illustration of major deuterostome relationships (branch lengths not proportional to evolutionary distance). Colored clades: deuterostomes. Grey branch: protostomes. (E) Tree (PHYML, LG + Γ) based on alignment of 102 deuterostome sequences, seven arthropod sequences (*Centruroides sculpturatus*, cyan) and 16 mollusk sequences (*Lottia gigantea*, green). No protostome (arthropod/mollusk) sequences appear in the ASIC clade (orange).

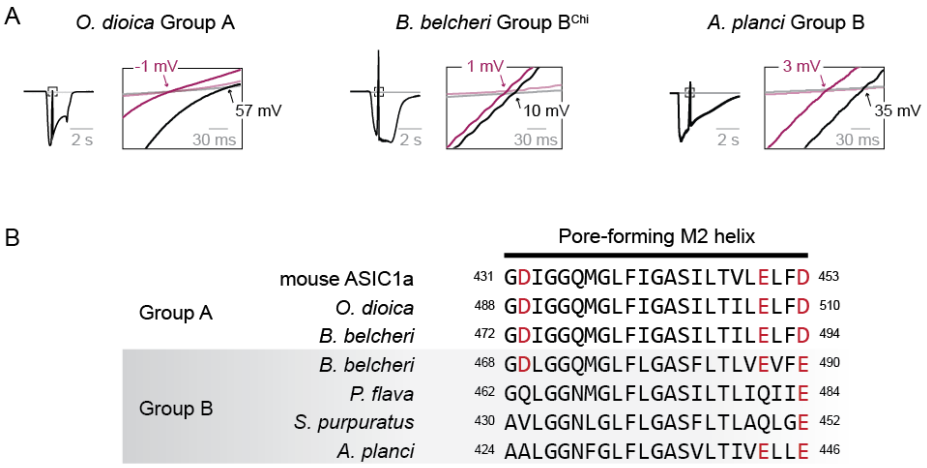

Fig. S2. Characterization of ASICs from non-vertebrate deuterostomes. (A) Recordings establishing reversal potential of proton-gated current. 200 ms voltage ramps from -60 mV to +60 mV were run during proton gated-current (bold traces, pH 6.0 for *O. dioica* A; pH 5.0 for *B. belcheri* B^{Chi}; pH 7.0 for *A. planci* B) and during rest (light traces, pH 7.5 for *O. dioica* A and *B. belcheri* B^{Chi}; pH 9.0 for *A. planci* B). The intersect of proton-gated and resting current traces yielded the reversal potentials (V_{rev}, indicated) with extracellular NaCl (black) or KCl (purple). These were used to calculate relative permeability P_{Na+}/P_{K+} with the Goldman-Hodgkin-Katz equation, $P_{Na+}/P_{K+} = \exp(F(V_{rev,Na+} - V_{rev,K+})/RT)$, where F = Faraday constant, R = gas constant, and T = 293 K. (B) Segment of amino acid sequence alignment of mouse ASIC1a and newly identified ASICs. Acidic residues implicated in ion conduction and/or selectivity are shown in red (8, 13).

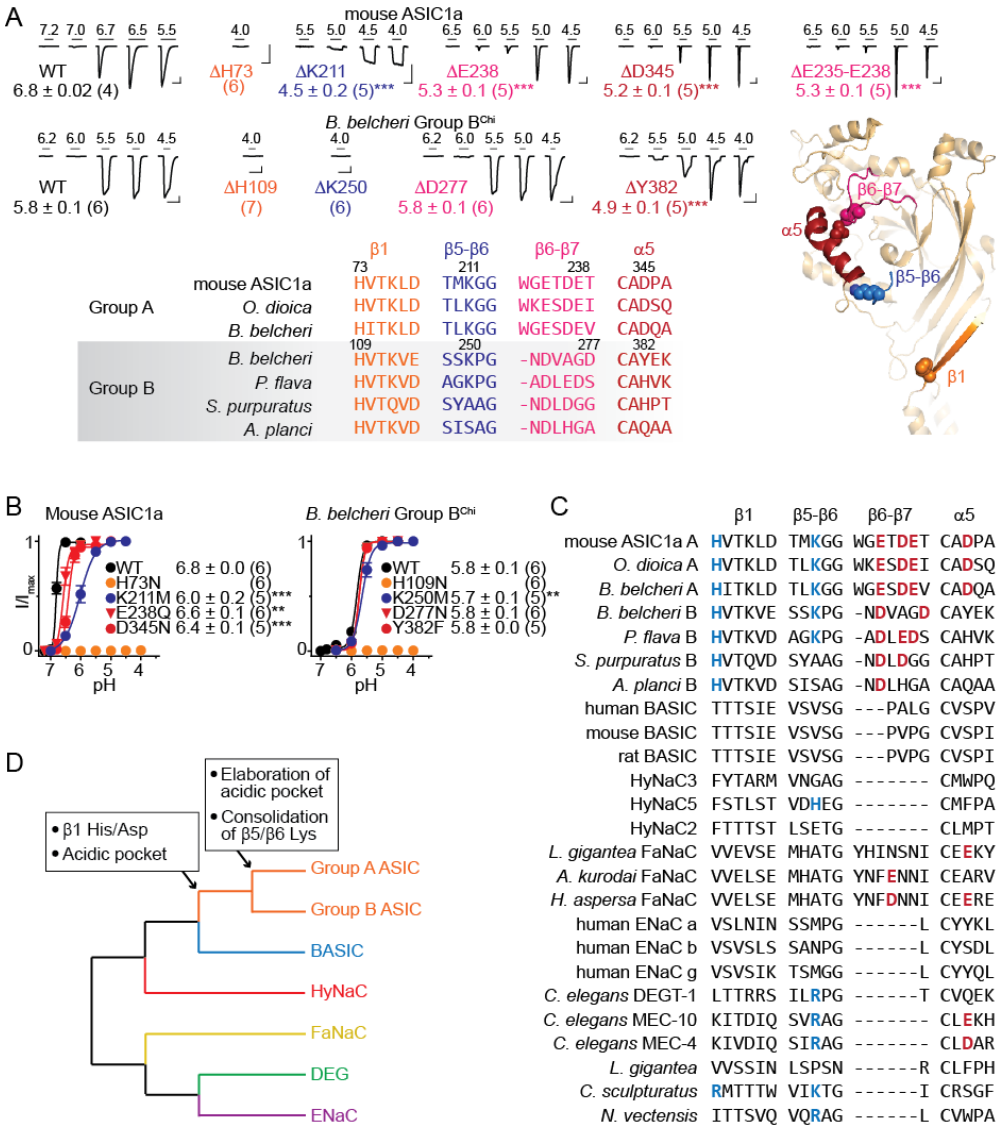

Fig. S3. Characterization of mutant ASICs. (A) Example recordings and amino acid sequence alignment. G276 in *B. belcheri* GroupB^{Chi} (≈E238 in mouse ASIC1a) has no side chain, therefore D277 was deleted instead. Scale bars: x 10s; y 1 μA, except ΔH73 and ΔH73, 0.5 μA. *Right*, chick ASIC1 subunit (PDB 2QTS) showing residues equivalent to mouse ASIC1a H73, K211, E238 and D345 in spheres; K211 (blue) is from an adjacent subunit. Mean (± SD) pH_{50} values indicated: ***P*<0.01, ****P*<0.001 compared to WT (one-way ANOVA with Dunnett's test). (B) Normalized peak current responses to decreasing pH for indicated ASIC1a or *B. belcheri* Group B^{Chi} ASIC mutants (mean ± SEM, n = 5-6). Mean (± SD) pH_{50} values indicated. (C) Alignment of these segments in broader DEG/ENaC family. Sequences retrieved from UniProt or NCBI blast searches. *L. gigantea* FaNaC refers to Genbank entry XP_009053562.1. *L. gigantea* (mollusk), *C. sculpturatus* (arthropod), *N. vectensis* (cnidarian) refer to Genbank entries XP_009051302.1, XP_023215424.1 and XP_001641515.1, respectively: these are included as the top hits for ASIC-like sequences from two non-deuterostome bilaterians and one cnidarian. (D) Cartoon showing DEG/ENaC relationships based on present and other (14) work, indicating the emergence of crucial amino acid changes. (Scale does not reflect evolutionary distance.)

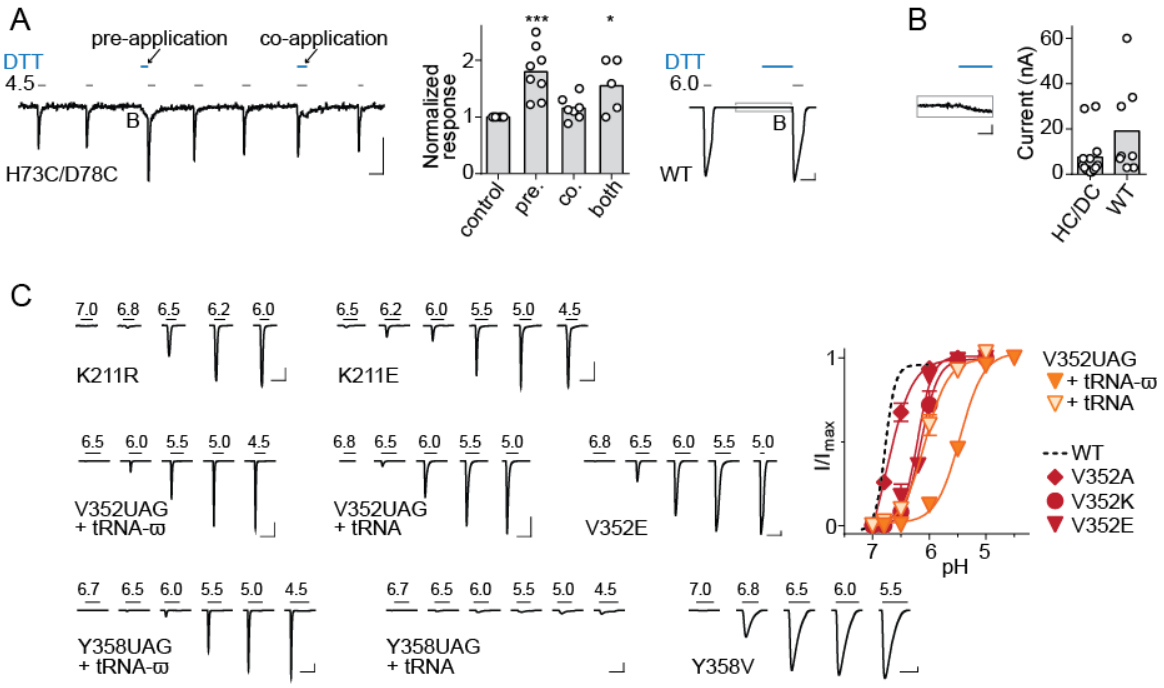

Fig. S4. Introduced cross-links and non-canonical amino acid incorporation in ASIC1a. (A) Example and average normalized current responses to pH 4.5 at mouse ASIC1a H73C/D78C-expressing oocytes, with application of 2 mM DTT before or during pH 4.5. WT control shown on right (pH 6.0 and 2 mM DTT). **P* = 0.018, ****P* = 0.0002, one-way ANOVA with Dunnett's comparison with control. Scale bars: x 10s; y 0.1 µA (H73C/D78C) and 1 µA (WT). "Both" refers to combined pre- and co-application (not illustrated here). "B" indicates DTT-induced current, addressed in (B). (B) Magnified version of WT recording in (A), and average current in response to 2 mM DTT. n = 14 (H73C/D78C) and 8 (WT), *P* = 0.083, Student's t-test). As DTT-induced current is statistically similar at H73/D78C and WT oocytes, it presumably does not derive from the C73/C78 link. Scale bars: x 10 s; y 0.1 µA. (C) Recordings from regular and nonsense suppression mutant constructs (scale bars: x 10 s; y 1 µA). For nonsense suppression, oocytes were co-injected with cRNA containing an amber stop codon at the position in question and non-canonical aminoacylated tRNA (e.g. "V352UAG + tRNA-ϖ"). After translation, the tRNA can in theory be used by the cellular machinery to non-specifically incorporate endogenous amino acids. As a control for this, co-injection of UAG cRNA and non-aminoacylated tRNA was tested (e.g. "V352UAG + tRNA"). For Y358, there was little, if any, non-specific incorporation (note minimal proton-gated currents for "Y358UAG + tRNA"). For V352, these control oocytes showed proton-gated currents, indicative of non-specific incorporation, and the proton sensitivity was similar to oocytes expressing regular V352E mutants (compare unfilled orange triangles with filled red triangles in concentration-response graph), possibly suggesting that the currents largely reflect incorporation of glutamic acid, the most abundant endogenous amino acid in *X. laevis* oocytes (15). None of the regular mutants tested, V352E, V352K or V352A, showed such a decrease in proton sensitivity as V352UAG + tRNA-ϖ (filled orange triangles in concentration-response graph), suggesting that successful incorporation of ϖ generates channels of low proton sensitivity.

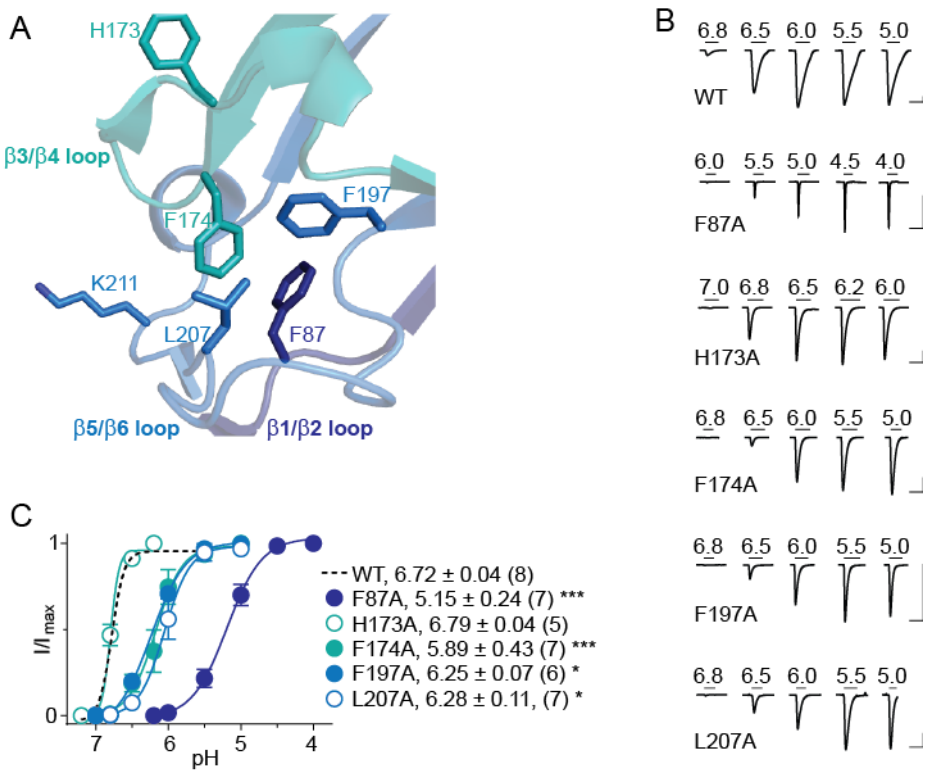

Fig. S5. Hydrophobic hub important for proton sensitivity in ASIC1a. (A) Chick ASIC1 X-ray structure (PDB 2QTS) showing hydrophobic side chains vicinal to K211. All numbers refer to equivalent residues from mouse ASIC1a. Mouse ASIC1a H173 (equivalent to F174 in chick ASIC1 at top of image) is the only divergent residue. (B) Example recordings from oocytes expressing indicated mouse ASIC1a constructs. Scale bars: x 10 s; y 1 µA. Oocytes injected with 40 ng cRNA (F87A and F197A) or 0.8 ng cRNA (all other constructs). 0.8 ng F87A and F197A cRNA yielded little proton-gated current (not shown). (C) Normalized peak current responses to decreased pH for indicated constructs (mean ± SEM, n = 5-8). Legend includes pH_{50} values (mean ± SD from (n) separate experiments); **P* < 0.05, ****P* < 0.001 in one-way ANOVA with Dunnett's Test comparing to WT value.

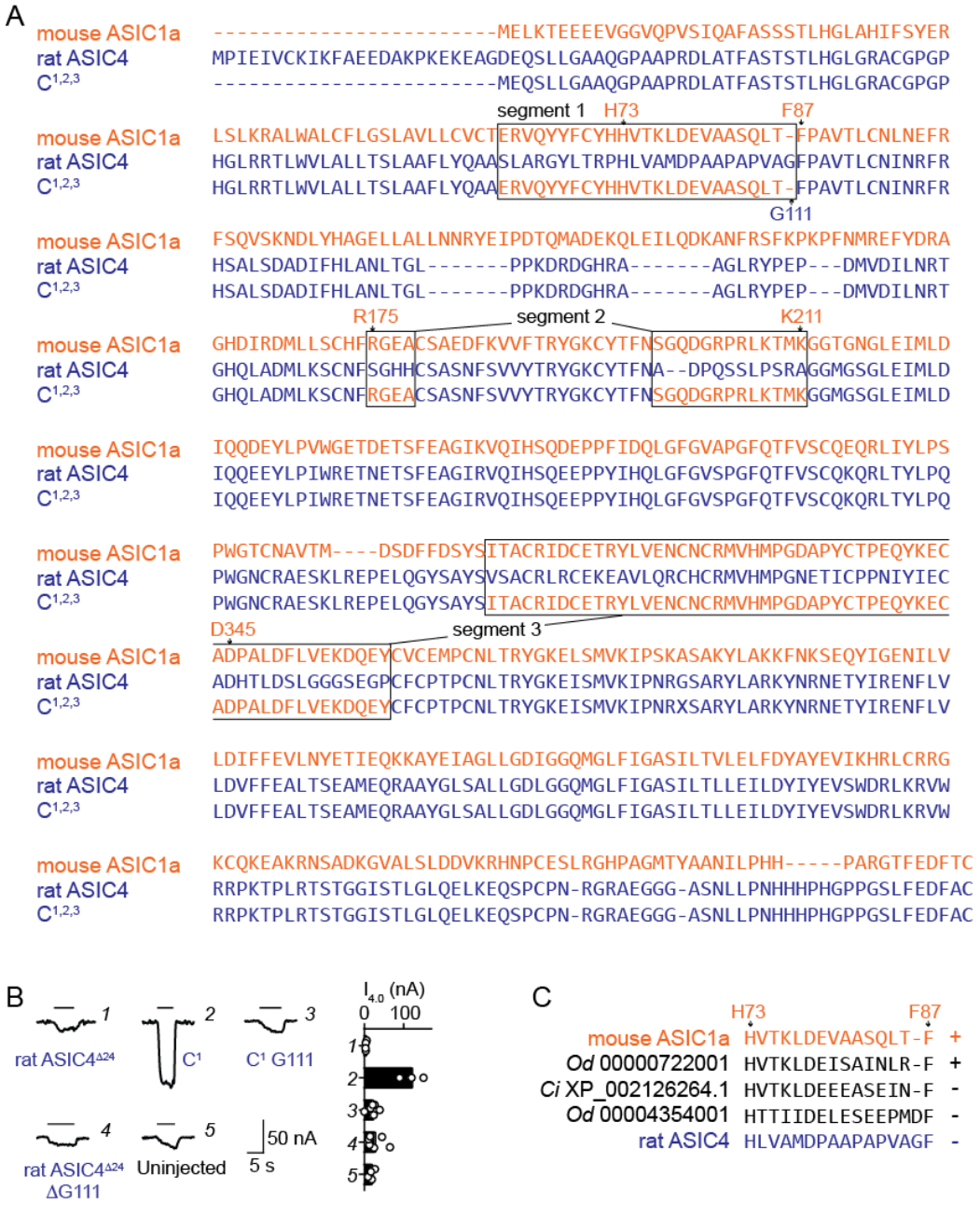

Fig. S6. Mouse ASIC1a/rat ASIC4 chimeras. (A) Amino acid sequence alignment of mouse ASIC1a, rat ASIC4 and chimera $C^{1,2,3}$ from the present study, illustrating the ASIC1a segments used for chimeras. Selected ASIC1a residues from these segments that contribute to proton sensitivity are indicated (present study; (16, 17)). Rat ASIC4 glycine residue also indicated (within segment 1). This glycine residue is conserved in mammalian ASIC4 but is absent in non-mammalian ASIC4 sequences. (B) Example and mean peak current responses to pH 4.0 (black bars) in oocytes expressing indicated constructs. "C^1" is the chimera containing mouse ASIC1a segment 1; "C^1 G111" is the same but with a glycine inserted into this segment. (C) Alignment including *Oikopleura dioica* ("*Od*") and *Ciona intestinalis* ("*Ci*") sequences. "+", proton-gated currents; "-" absence of proton-gated currents (present study and ref. (18)).

References

1. Katoh K, Misawa K, Kuma K, & Miyata T (2002) MAFFT: a novel method for rapid multiple sequence alignment based on fast Fourier transform. *Nucleic Acids Res* 30(14):3059-3066.
2. Guindon S & Gascuel O (2003) A simple, fast, and accurate algorithm to estimate large phylogenies by maximum likelihood. *Syst Biol* 52(5):696-704.
3. Cannon JT, *et al.* (2016) Xenacoelomorpha is the sister group to Nephrozoa. *Nature* 530(7588):89-93.
4. Price MN, Dehal PS, & Arkin AP (2010) FastTree 2--approximately maximum-likelihood trees for large alignments. *PLoS One* 5(3):e9490.
5. Kearse M, *et al.* (2012) Geneious Basic: an integrated and extendable desktop software platform for the organization and analysis of sequence data. *Bioinformatics* 28(12):1647-1649.
6. Molday LL & Molday RS (2014) 1D4: a versatile epitope tag for the purification and characterization of expressed membrane and soluble proteins. *Methods Mol Biol* 1177:1-15.
7. Lynagh T, Komnatnyy VV, & Pless SA (2017) Unique Contributions of an Arginine Side Chain to Ligand Recognition in a Glutamate-gated Chloride Channel. *J Biol Chem* 292(9):3940-3946.
8. Lynagh T, *et al.* (2017) A selectivity filter at the intracellular end of the acid-sensing ion channel pore. *Elife* 6.
9. Dahan DS, *et al.* (2004) A fluorophore attached to nicotinic acetylcholine receptor beta M2 detects productive binding of agonist to the alpha delta site. *Proc Natl Acad Sci U S A* 101(27):10195-10200.
10. Mikhaleva Y, Kreneisz O, Olsen LC, Glover JC, & Chourrout D (2015) Modification of the larval swimming behavior in Oikopleura dioica, a chordate with a miniaturized central nervous system by dsRNA injection into fertilized eggs. *J Exp Zool B Mol Dev Evol* 324(2):114-127.
11. Canessa CM, Horisberger JD, & Rossier BC (1993) Epithelial sodium channel related to proteins involved in neurodegeneration. *Nature* 361(6411):467-470.
12. Wiemuth D, Assmann M, & Grunder S (2014) The bile acid-sensitive ion channel (BASIC), the ignored cousin of ASICs and ENaC. *Channels (Austin)* 8(1):29-34.
13. Yang L & Palmer LG (2014) Ion conduction and selectivity in acid-sensing ion channel 1. *J Gen Physiol* 144(3):245-255.
14. Assmann M, Kuhn A, Durrnagel S, Holstein TW, & Grunder S (2014) The comprehensive analysis of DEG/ENaC subunits in Hydra reveals a large variety of peptide-gated channels, potentially involved in neuromuscular transmission. *BMC Biol* 12:84.
15. Taylor PM, Kaur S, Mackenzie B, & Peter GJ (1996) Amino-acid-dependent modulation of amino acid transport in Xenopus laevis oocytes. *J Exp Biol* 199(Pt 4):923-931.
16. Gwiazda K, Bonifacio G, Vullo S, & Kellenberger S (2015) Extracellular Subunit Interactions Control Transitions between Functional States of Acid-sensing Ion Channel 1a. *J Biol Chem* 290(29):17956-17966.
17. Paukert M, Chen X, Polleichtner G, Schindelin H, & Grunder S (2008) Candidate amino acids involved in H+ gating of acid-sensing ion channel 1a. *J Biol Chem* 283(1):572-581.
18. Coric T, Passamaneck YJ, Zhang P, Di Gregorio A, & Canessa CM (2008) Simple chordates exhibit a proton-independent function of acid-sensing ion channels. *FASEB J* 22(6):1914-1923.